CW Emission and Self-Pulsing in a III-V/SiN Hybrid Laser With Narrow Band Mirror

Cristina Rimoldi ⬡ , *Member, IEEE*, Lorenzo L. Columbo ⬡ , *Member, IEEE*, Jock Bovington ⬡ , *Member, IEEE*, Sebastian Romero-García ⬡ , and Mariangela Gioannini ⬡ , *Member, IEEE*

Abstract—We report on how external cavity III-V/SiN hybrid lasers operate in regimes of ultra-damped relaxation oscillations or in CW unstable dynamical regimes (self-pulsing or approaching turbulence) as a consequence of mirror dispersion, non-zero linewidth enhancement factor, and four-wave mixing in the gain medium. The impact of the dispersive mirror bandwidth and different mirror effective lengths on the laser tolerance to external optical feedback is also discussed.

Index Terms—Four wave mixing, modeling, nonlinear optical effects in semiconductors, optical interconnects, semiconductor lasers.

I. INTRODUCTION

IN RECENT years silicon photonics platforms have been attracting surging interest from industries [1] for their application in the context of transmitters in optical communications, as well as in the context of sensing and LIDAR. Here, the integration of laser sources represents one of the main challenges towards commercialization, despite the several recent technological advancements. Laser sources integrated in SiPh platforms (either through flip-chip bonding or heterogeneous integration) consist of III-V gain materials coupled to the rest of the SiPh circuit, providing the mirror to form the external laser cavity. Several solutions have been achieved through the design of SiPh chips for the realization of external cavities with long effective lengths, supplying wide tunability as well as narrow laser linewidths [2]–[4]: these include but are not limited to the use of combined passive components such as delay lines, microrings, and DBR reflectors. Several studies have been dedicated to the achievement of very narrow laser linewidth, both from an experimental and a theoretical point of view [5]. On the other hand, few works have focused on the characterization of CW instability and the dynamical regimes that emerge from it. Here, we consider a hybrid laser design based on our work in [6]. Based on [6], the design consists in optimized ring coupling coefficients

such that we can achieve at same time narrow laser linewidth (<100 kHz), good WPE (about 20%), and output power of 20 mW at the acceptable cost of RSOA bias current less than 200 mA. In the present paper, we theoretically address the impact of a dispersive narrow band reflector on the laser dynamical performance and the occurrence of multi-mode regimes. Similar regimes have been experimentally observed in extended DBR lasers [4] and other hybrid lasers [7]; in particular [7] reports a self-pulsing comb regime, attributed to the mode beating of two longitudinal cavity modes. To the best of our knowledge, these regimes still lack a detailed theoretical explanation of the physical mechanism lying behind their formation. This paper is based on the approach we developed in [8] of which it extends the results and understanding. The first aim of this work is focusing more on the analysis of the CW instability by showing that we can reproduce and explain experimental results similar to those recently reported in [4], [7] where self-pulsing and turbulent regimes were found by detuning the lasing frequency with respect to the effective reflectivity peak. In this work we explain that these multi-mode regimes are the consequence of the interplay of three coexisting mechanisms: i) the non-null RSOA Linewidth Enhancement Factor (LEF) that, together with ii) the narrow band mirrors, turns the laser frequency noise into non-negligible intensity noise that may trigger multimode emission, and iii) the Four-Wave Mixing (FWM) which enhances the parametric gain of the cavity longitudinal modes adjacent to the lasing one [9]. As a second aim we analyze in more detail with respect to [8] the sensitivity of these lasers to the external optical feedback by comparing two hybrid laser designs in section IV: i) a design obtained by narrowing the bandwidth of the silicon photonic mirror and hence increasing the effective lengths of the external cavity and ii) a design, similar to [8], with different bandwidth of the effective mirror but same effective cavity lengths. While design (ii) serves to understand the impact of the sole effective mirror bandwidth on the external feedback tolerance, design (i) is more realistic (being closer to practical laser realizations) and allows also to address the role of the effective length on the laser CW stability. While the presented results focus on a specific hybrid laser configuration (where the narrow band reflection is provided by two coupled micro-rings), the achieved results can be applied to a wider range of design choices, relying for example on narrow band reflectors realized with low-k DBRs [10]. The paper is organized as follows: in Section II we present the considered hybrid laser configuration

Cristina Rimoldi, Lorenzo L. Columbo, and Mariangela Gioannini are with the Dipartimento di Elettronica e Telecomunicazioni, Politecnico di Torino, 10129 Torino, Italy (e-mail: cristina.rimoldi@polito.it; lorenzo.columbo@polito.it; mariangela.gioannini@polito.it).

Jock Bovington and Sebastian Romero-García are with Cisco Optical, 90411 Nuremberg, Germany (e-mail: jbovingt@cisco.com; sromerog@cisco.com).
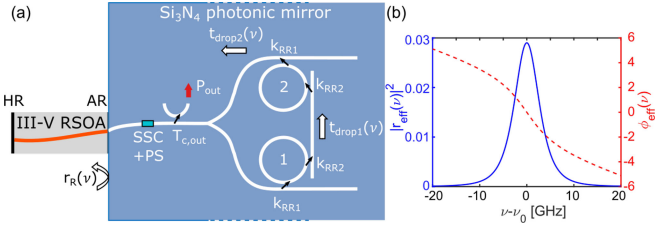
(a)

(b)

Fig. 1. (a) Schematic of the hybrid laser structure. (b) Effective reflectivity in modulus square (left y-axis) and phase (right y-axis) versus frequency for FWHM=6.2 GHz.

and the numerical model used for its description (based on [9] and presented in detail in [8]). In Section III we show the solitary laser numerical results and the observed multi-mode regimes and give an explanation for their occurrence. Further, we demonstrate the damping of relaxation oscillations in some specific configurations, which we study in detail in terms of resilience to spurious back-reflections in Section IV. In particular, we analyze the impact of external optical feedback and its dependence on the dispersive mirror bandwidth and laser effective length and we show that where relaxation oscillations are strongly damped, photon-photon resonance becomes the main cause of instability in presence of feedback.

II. HYBRID LASER CONFIGURATION AND MODELING

In Fig. 1(a) we show the hybrid laser configuration considered throughout the paper. This laser consist of an off-the-shelf III-V MQW 1 mm long HR/AR Reflective Semiconductor Optical Amplifier (RSOA) edge-coupled to a SiPh circuit based on two coupled Si_3N_4 micro-rings, which provide narrow band dispersive reflectivity through Vernier effect. The ring radii R_1 and R_2 (≈ 100 μm) are finely selected in order to maximize the tuning range and minimize the overlap of the ring resonance peaks near the lasing one. The ring coupling coefficients k_{RR1} and k_{RR2} are chosen as equal in order to obtain maximum mirror reflectivity in the critical coupling regime. The peak of $|r_R(\nu)|^2$ is 3% and the effective reflectivity of the SiPh mirror has a bandwidth of 6 GHz (unless otherwise specified), obtained through ring design. The output power P_{out} is collected through the output coupler $T_{c,out} = 73\%$, the value of which is chosen to maximize Wall-Plug Efficiency at $P_{out} = 20$ mW [6]. The arms between the splitter and the rings, the straight waveguide coupling the two rings, and the straight waveguide between the Spot Size Converter (SSC) and the splitter are approximately 500 μm, 300 μm, and 1 mm respectively, with specific values depending on the ring radii optimization. We report in Table I the parameters of the III-V RSOA and the SiPh mirror. Tuning of the phase $\Delta\phi$ of the control section PS allows for the detuning of the lasing frequency with respect to the effective reflectivity peak. Assuming a Lorentzian response for the rings around the reference frequency and that the two rings are tuned to align both ring resonance angular frequencies at ω_0, the reflection coefficient at the right facet of the RSOA, indicated here as $r_R(\omega)$, is equal to the reflection coefficient, indicated as $r_{eff}(\omega)$, of the SiPh mirror in the blue area of Fig. 1(a). More in general $r_R(\omega)$ must account for both the SiPh mirror and for any external

TABLE I
HYBRID LASER PARAMETERS

SiPh mirror parameters	
SSC insertion loss	2 dB
Waveguide effective refractive index	$n_{eff,SiN} = 1.55$
Waveguide group refractive index	$n_{g,SiN} = 1.76$
Power output coupler coefficient	$T_{c,out} = 0.73$
SOA parameters	
HR facet reflection coefficient	$r_1^2 = 0.9$
Internal quantum efficiency	$\eta_i = 0.76$
Length	$L = 0.1$ cm
Active region volume	$V = 1.5 \times 10^{-10}$ cm^3
Effective refractive index	$n_{eff} = 3.5$
Group refractive index	$n_g = 3.8$
Internal loss	$\alpha_i = 7.6$ cm^{-1}
Linewidth enhancement factor	$\alpha = 3$
Carrier lifetime	$\tau_N = 1$ ns
Transparency carrier density	2.1×10^{17} cm^{-3}
Modal gain coefficient	$g_N = 38$ cm^{-1}
Carrier reference wavelength	$\lambda_0 = 1.31$ μm

optical feedback intended as a fraction of the output power (P_{out} in Fig. 1(a)) reflected by a spurious back reflection from a distance L_{ext} from the output port. Without this spurious back reflection, $r_R(\omega)$ can be written as

$$r_R(\omega) = r_{eff}(\omega)$$

$$= \frac{\gamma_{c1}\gamma_{c2}t_{SSC}^2(1 - T_{c,out})}{(\gamma_{t1} + i\Delta\omega)(\gamma_{t2} + i\Delta\omega)}e^{-i\Delta\phi}e^{-i\Delta\omega\tau_{in,SiN}} \quad (1)$$

where $\omega = 2\pi\nu$, t_{SSC} is the SSC transmission coefficient, $\tau_{in,SiN}$ is the time delay due to the path in the straight waveguide parts of the SiPh circuit (SSC, phase section, splitter, etc.), and $\Delta\omega = \omega - \omega_0$, with ω_0 reference angular frequency. The coefficients $\gamma_{c1,2}$, $\gamma_{t1,2}$ respectively define the coupling rate of the electric field into the ring from the bus waveguide and the rate at which the electric field from the ring is lost, due to waveguide loss and coupling out of the bus waveguide. In particular [11]

$$\gamma_{c1,2} = \frac{v_{g1,2}k_{RR}^2}{2\pi R_{1,2}T_{RR}A_{loss1,2}^{1/4}} \quad (2a)$$

$$\gamma_{t1,2} = \frac{v_{g1,2}\left(1 - T_{RR}A_{loss1,2}^{1/2}\right)}{2\pi R_{1,2}T_{RR}A_{loss1,2}^{1/2}} \quad (2b)$$

with $T_{RR} = 1 - k_{RR}^2(1 - \eta)$, $A_{loss1,2}$ being the ring losses and η being the power coupling loss. A graph of the modulus square and phase of $r_R(\nu)$ in (1) is shown in Fig. 1(b) for a specific choice of $\gamma_{c1,2}, \gamma_{t1,2}$, resulting in an effective reflectivity bandwidth of $|r_{eff}|^2$ of 6.2 GHz and corresponding to a power coupling coefficient $k_{RR}^2 = 0.1$ in the ideal case of $\eta = 0$ and negligible losses in the bent waveguides (given the small value of the ring radii).

To account for spurious optical back-reflection, in Section IV we will include an external reflector r_{ext} placed at a distance L_{ext} from the output coupler. In this case the expression for the reflectivity $r_R(\omega)$ becomes

$$r_R(\omega) = r_{eff}(\omega) + t_{SSC}^2 T_{c,out}r_{ext}e^{-i\phi_{ext}}e^{-i\tau_{ext}\Delta\omega} \quad (3)$$

with $r_{eff}(\omega)$ identifying the contribution to the reflectivity related to the two coupled rings, $\phi_{ext} = 2L_{ext}\omega_0 n_{eff,SiN}/c$ with $n_{eff,SiN}$ effective refractive index of the SiN waveguide, and τ_{ext} external cavity delay. The effective length of the SiPh mirror is determined as $L_{eff} = -(v_{g,SiN}/2)\partial\phi_{eff}(\omega)/\partial\omega|_{\omega=\omega_0}$, with $v_{g,SiN}$ group velocity in the SiPh circuit and will be a relevant parameter in the study of the laser tolerance to optical feedback. Additional details regarding this hybrid laser configuration are given in [6], [8]. The model developed to describe the hybrid laser dynamics is based on the approach reported in [9] and detailed in [8]. It consists in a set of time-delayed algebraic differential equations at the reference plane of the AR-coated facet of the RSOA. In particular, we couple an evolution equation for the slowly varying envelope of the electric field $E(t)$, exiting the SOA at the AR-coated facet and incident on the SiPh mirror, to a differential equation for the envelope $A_{c1}(t)$ of the electric field out of the drop port of ring 1, a differential equation for the envelope $A_{c2}(t)$ of the electric field after propagation in ring 2, the splitter, PS, and SSC, and a standard differential equation for the carrier density $N(t)$. The resulting set of equations is

$$E(t) = \frac{e^{i(\omega_s-\omega_0)\tau_{in}} \exp\left(f(\omega_s, N_s)\right)}{r_R(\omega_s)} A^-(t - \tau_{in}) + F(t) \tag{4a}$$

$$\dot{A}_{c1}(t) = \gamma_{c1} t_{SSC}^2 (1 - T_{c,out}) E(t - \tau_{in,SiN}) e^{-i\Delta\phi}$$
$$- \gamma_{t1} A_{c1}(t) \tag{4b}$$

$$\dot{A}_{c2}(t) = \gamma_{c2} A_{c1}(t) - \gamma_{t2} A_{c2}(t) \tag{4c}$$

$$\dot{N}(t) = \frac{\eta_i I_{bias}}{qV} - \frac{N(t)}{\tau_N} - v_g g_N \ln\left(\frac{N(t)}{N_0}\right) \sigma \frac{|E(t)|^2}{V} \tag{4d}$$

with $A^-(t)$ such that

$$A^-(\omega - \omega_0) = r_R(\omega) E(\omega - \omega_0) \tag{5}$$

and

$$f(\omega_s, N_s) = \frac{1}{\tau_{in}} \int_{t-\tau_{in}}^{t} L\left(1 + i\alpha\frac{\omega_s}{\omega_0}\right) g_N \ln\left(\frac{N(\bar{t})}{N_s}\right) d\bar{t} \tag{6}$$

Note that in absence of external optical feedback $A^-(\Delta\omega) = A_{c2}(\Delta\omega) = r_{eff}(\omega)E(\Delta\omega)$, while, when $r_{ext} \neq 0$, it includes also the contribution of the envelope of the electric field from the external reflector. Differently from the effective Lang-Kobayashi approach presented in [6], this model allows to account for the frequency-selective mirror and is suitable to analyze the laser dynamics for SiPh mirror reflection coefficient bandwidths varying from a few GHz (≤ 1 GHz) to several GHz (>11 GHz) [8]. The term $F(t)$ in (4a) accounts for spontaneous emission noise as in [9]. In particular, $F(t) = \sqrt{\beta_{sp} h\nu_s R_{sp}} \exp(i\phi_{rand}(t))$, where R_{sp} is the total spontaneous recombination rate, β_{sp} is the fraction of spontaneous emission coupled into the lasing mode, $\nu_s = \omega_s/2\pi$ is the lasing frequency, h is the Planck constant, and $\phi_{rand}(t)$ is a random phase term. The linewidth enhancement factor is α and τ_{in} is the RSOA cavity roundtrip time. Eq. (4d) accounts for the spatially averaged carrier density in the RSOA. Here, η_i is the internal

quantum efficiency, I_{bias} is the bias current, v_g is the group velocity within the RSOA, V is the volume of the active region, N_0 is the carrier density at transparency, and q is the electron charge. Finally, g_N is the modal gain coefficient (including the optical confinement factor in the transverse plane), and σ is a coefficient dependent on the CW solution, accounting for the average of the electric field along propagation through the RSOA, defined such that $\sigma|E|^2/V$ is the photon density per unit volume in the RSOA. More details on the derivation of this coefficient can be found in [8], [9], [12]. Optical propagation losses in the straight SiN waveguides are assumed to be small in comparison with the SSC insertion loss and are therefore neglected.

The model in (4a)–(4d) allows for a linear stability analysis (LSA) in the frequency domain [8] of the lasing mode solution ω_s: the eigenvalues $\lambda = i\tilde{\omega}$ of the resulting linear system of perturbations, as we will see in the following Section, are associated to relaxation oscillations (RO) and photon-photon resonance (PPR). Each eigenvalue has an associated perturbation oscillation frequency (imaginary part of λ) and a perturbation damping factor (real part of λ or perturbation growth rate). The laser becomes unstable if at least one of the eigenvalues has a negative damping factor (i.e., the perturbation growth rate becomes positive). In the following Sections, we utilize the results of the LSA to address the physical causes of CW instability both in the solitary laser regime and in presence of external optical feedback. We show that in some cases, depending on the detuning of lasing frequency with respect to ω_0, the CW instability of the solitary laser can lead to self-pulsing.

III. DYNAMICAL STUDY OF THE SOLITARY LASER

Fig. 2(a) shows the map of the integrated Relative Intensity Noise (RIN), over a bandwidth of 25 GHz, resulting from dynamical simulations of the solitary laser ($r_{ext} = 0$) through (4a)–(4d) for an effective reflectivity $|r_{eff}(\nu)|^2$ bandwidth of 6.2 GHz, 30 increasing values of RSOA bias current (from 20 mA to 250 mA), and 30 different values of detuning $\Delta\nu$ of the lasing frequency with respect to ω_0, obtained by sweeping the phase shift parameter $\Delta\phi$ of the phase control section PS. The effective length corresponding to this reflectivity bandwidth is $L_{eff} = 0.73$ cm. The blue region of low RIN (<-160 dBc/Hz) identifies a stable single-mode regime, while the red region of high RIN (>-130 dBc/Hz) corresponds to a multi-mode regime, which can be characterized by a self-pulsing or turbulent behavior, as we will see in the following. The white dashed line is the result of LSA and highlights the border of CW (single-mode) instability. The inset in Fig. 2(a) displays an example of the self-pulsing time trace of the output power in the CW unstable region at the point highlighted by the white arrow that corresponds to $\Delta\nu = -4.24$ GHz and $I_{bias} = 202$ mA.

In order to address the cause of CW instability we focus on a specific value of frequency detuning, i.e. $\Delta\nu = -4.24$ GHz, and we report in Fig. 2(b) a map of the RIN spectra obtained by varying the bias current (matching the parametric region identified by the black vertical line in Fig. 2(a)). For this value
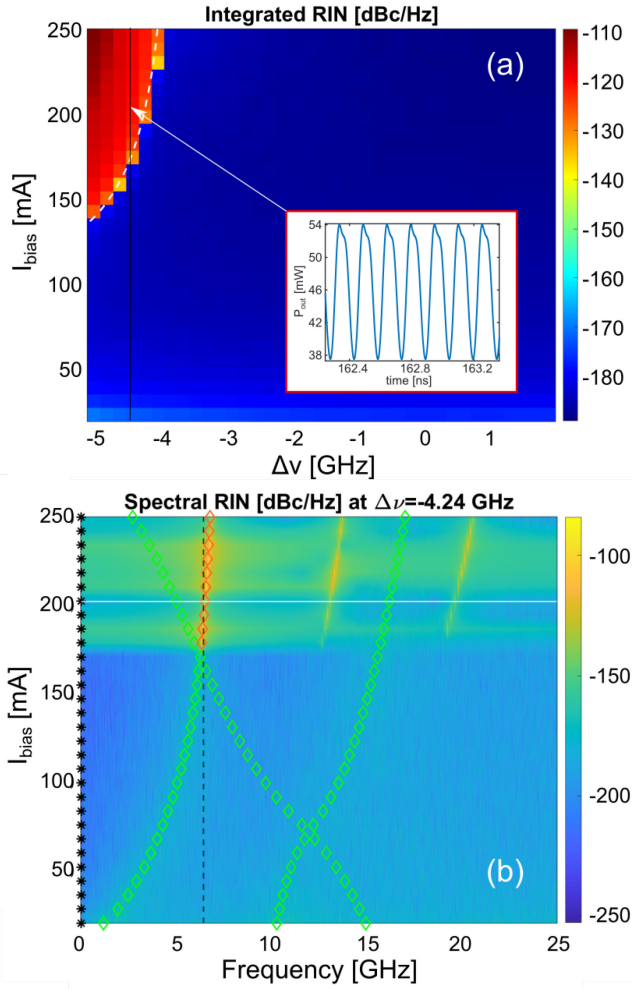
Fig. 2. (a) Integrated RIN map computed over a bandwidth of 25 GHz for different values of bias current and detuning of the lasing frequency at $|r_{eff}|^2$ FWHM=6.2 GHz. The white dashed line highlights the border of instability. The inset shows a typical time trace of the output power in the parametric region highlighted by the white arrow ($\Delta\nu = -4.24$ GHz and $I_{bias} = 202$ mA). (b) Map of the RIN spectra for different values of bias current at $\Delta\nu = -4.24$ GHz (corresponding to the the black vertical line in (a)). Green (orange) diamond markers identify the system eigenvalue frequencies when the perturbation damping is positive (negative). The black vertical dashed line highlights the beating between the lasing mode and another longitudinal cavity mode. The white horizontal line simply identifies the RIN spectrum matching the inset temporal trace in (a).

of $\Delta\nu$, single-mode emission becomes unstable for $I_{bias} > 170$ mA as shown by the sudden increase of the RIN. The green and orange diamond markers show the perturbation oscillation frequency associated to each eigenvalue from LSA in the considered frequency range. At low currents all eigenvalues have positive damping and are therefore marked as green, when one of the eigenvalues starts to have negative damping, it is marked in orange. The first eigenvalue, growing monotonically in frequency (from ≈0 GHz at threshold to ≈6 GHz at $I_{bias} = 250$ mA) for increasing values of current, is associated to relaxation oscillations [8]. The other two eigenvalues are instead associated to the photon-photon resonance resulting from the beating between the lasing mode and an adjacent cavity longitudinal mode [8], [13]. The eigenvalue associated to relaxation

oscillations is the one that gives eventually rise to instability when it becomes resonant with the beating frequency (highlighted by the black vertical dashed line) at 6.3 GHz between the lasing mode and another longitudinal mode at a higher threshold. At this point the eigenvalue starts to have a positive perturbation growth rate thus triggering a self-pulsing regime. The comb line separation in the self-pulsing regime is therefore approximately given by the frequency of relaxation oscillations. The white horizontal line in Fig. 2 identifies the RIN spectrum for the value of bias current $I_{bias} = 202$ mA that corresponds to the temporal trace of the output power reported in the inset of Fig. 2(a).

We now focus on the laser behavior at high currents, in order to further characterize the other dynamical regimes observed when single-mode emission becomes unstable. In Fig. 3(a) we report, in orange, how the lasing frequency $\Delta\nu$ varies with the phase shift $\Delta\phi$ introduced via the phase control section. We also report, in blue, the average output power observed in each corresponding dynamical simulation at $I_{bias} = 240$ mA. We can distinguish 3 main laser parametric regions, characterized by different dynamical behaviors and matching the optical spectra reported at the bottom of Fig. 3: in region (1) the laser is highly detuned and displays a regime approaching turbulence, region (2) displays a self-pulsing regime characterized by a frequency comb, and region (3) shows stable single mode emission. Comparable regimes have been experimentally observed in similar hybrid laser configurations [7] and extended DBR lasers [4], where they have been ascribed to mode competition. Here, we show in detail that similar self-pulsing regimes can be obtained as a result of the interplay of several physical mechanisms. To analyze the transition between single mode and multi-mode regimes, we consider in more detail the results of LSA, reported in Fig. 3(b). Here, we show with a blue solid line the damping rate (b) of the eigenvalue associated to relaxation oscillation, i.e. the one that gives rise to the CW instability. For negative detuning of the lasing frequency $\Delta\nu$, the phase noise, caused by spontaneous emission and the non-null LEF, turns into intensity noise due to the narrow band reflector and may cause another longitudinal mode to reach the lasing threshold. In particular, when the beating frequency between neighboring modes becomes resonant with relaxation oscillations, the latter become undamped triggering the CW instability. If this occurs for sufficiently high bias current, i.e. high intracavity field power, the nonlinear FWM phenomenon is efficient in providing mode proliferation through parametric gain and phase-locking that lead to a self-pulsing regime (region 2). For further (negative) detuning of the lasing frequency multi-mode competition gives rise to a more complex regime, approaching turbulence (region 1), typically characterized by an enlargement of the optical spectrum due to the transfer of energy (cascading) to larger frequencies without locking. This effect leading to self-pulsing tends instead to decrease for smaller (but still negative) detuning, because of the single mode stabilization mechanism of detuned loading [5], [14]: as a result, the perturbation is highly damped for an optimal value of (negative) detuning. The following reduction of damping towards positive detunings is due to the progressive reduction of the detuned loading effect. As illustrated in light-blue solid line in Fig. 3(b), this scenario
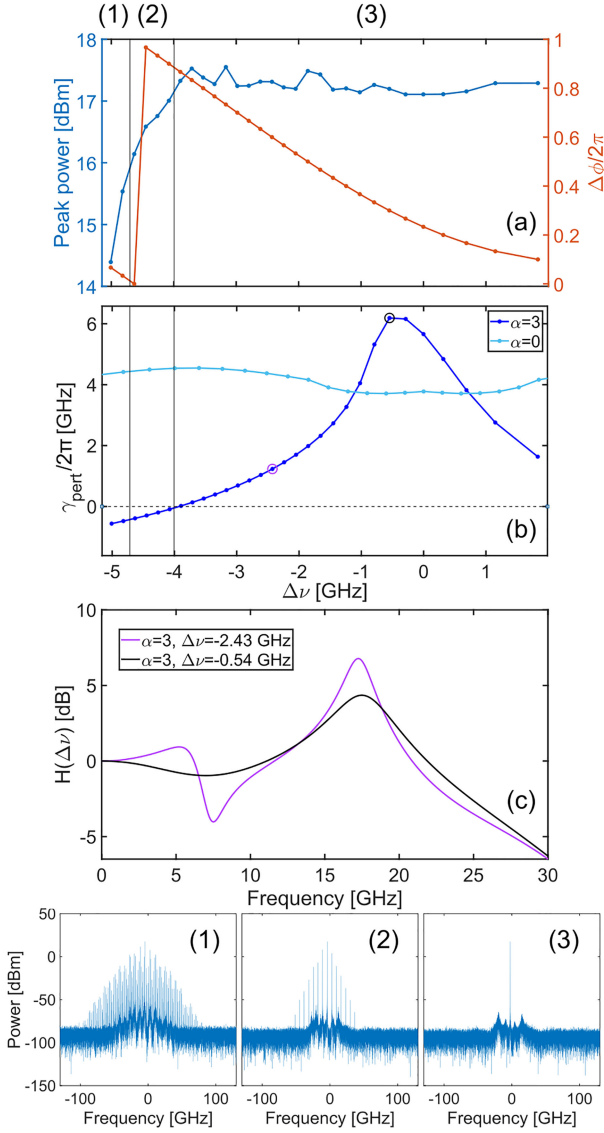
Fig. 3. (a) Lasing frequency (orange) and output power (blue) obtained through tuning of the phase section PS. (b) damping γ_{pert} of the perturbation associated to ROs for varying values of lasing frequency for $\alpha = 3$ and, for comparison, for $\alpha = 0$. (c) Intensity-modulation response for a value of detuning of the lasing frequency at the peak of the perturbation damping (black line) and at a more negative value (violet), matching the circles of the same color in (b). (1-3) Optical spectrum examples, matching the parametric regions indicated in (a), calculated for $\beta_{sp} \approx 10^{-4}$. The bias current is fixed at 240 mA.

is completely altered when the effect of the LEF is neglected because of a reduced phase amplitude coupling: in this case (α=0) the self-pulsing (and quasi-turbulent) regimes are not observed. In Fig. 3(c) we show the Intensity-Modulation (IM) response obtained through dynamical simulations of (4a)–(4d) for lasing at the peak of damping of the eigenvalue associated to ROs (black line, corresponding to the black circle in Fig. 3(b)). In this configuration the only visible peak in the IM response is due to PPR at ≈ 17 GHz (for the sake of clarity the damping of the corresponding eigenvalue is not shown in Fig. 3(b)). Larger detuning of the lasing frequency towards negative values (e.g, at the point highlighted by the violet circle in Fig. 3(b)) imply less damping of ROs and the consequent emergence of a peak
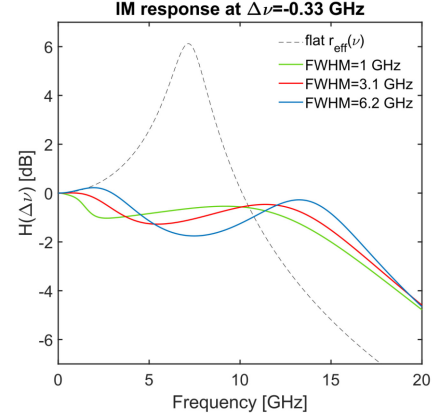

Fig. 4. Intensity-modulation response obtained through numerical integration of (4a)–(4d) at I_{bias}=104 mA and lasing frequency $\Delta\nu$=−0.33 GHz for different choices of reflectivity FWHM. The black dashed lines shows the corresponding IM response for $\alpha = 0$ in a single-mode laser [15].

in the IM response at ≈ 5 GHz. These results can exemplify a valuable approach for the interpretation of similar experimental findings [4], [7]. Finally, we analyze the IM response obtained for different choices of SiPh mirror reflectivity bandwidths. Considering recent developments in the realization of integrated lasers with very narrow reflectivity bandwidths [10], [16], [17], we compare results obtained for mirror bandwidth as small as 1 GHz. In Fig. 4, we show the IM response for $|r_{eff}(\nu)|^2$ FWHM of 1 GHz (in green), 3.1 GHz (in red), and 6.2 GHz (in blue) at $I_{bias} = 104$ mA and lasing frequency $\Delta\nu = -0.33$ GHz (i.e., near to the $|r_{eff}(\nu)|^2$ peak). The low frequency peak in the IM response is the one associated to RO [8]. As a general trend, Fig. 3 suggests that proper design of the SiPh effective mirror allows to obtain higher damping factors for narrower mirror bandwidths, in particular with respect to broadband reflectivities in single-mode lasers (see black dashed line) [15], which is in accordance with what has been predicted theoretically for Fano lasers in [18]. As also observed in Fig. 3(c), the longer cavity effective length implies the emergence of a second peak in the IM response, associated to PPR [13], which plays an important role in the laser tolerance to optical feedback.

IV. OPTICAL FEEDBACK TOLERANCE

The integration of lasers in silicon photonic PIC is an important challenge due to the very difficult integration of an optical isolator. To the best our knowledge there are no experimental data and measurements about the maximum tolerated feedback of this external cavity integrated laser and, for this reason, it is beneficial to analyze, at least at the theoretical and numerical level, the potential of these lasers for isolator-free operation [19], [20]. Several experimental data are instead available about tolerance to external feedback of DFB lasers. Reportedly, DFB lasers can stand up to −20 dB of external feedback as recently measured by Tang *et al.* [21] when applying a self-injection scheme with high-Q silicon micro-ring to increase the feedback tolerance to about −5 dB with a view to the integration in a silicon PIC. Less recently, M. Matsuda *et al.* [22] have reported QW-DFB feedback tolerance up to about -16 dB, showing that
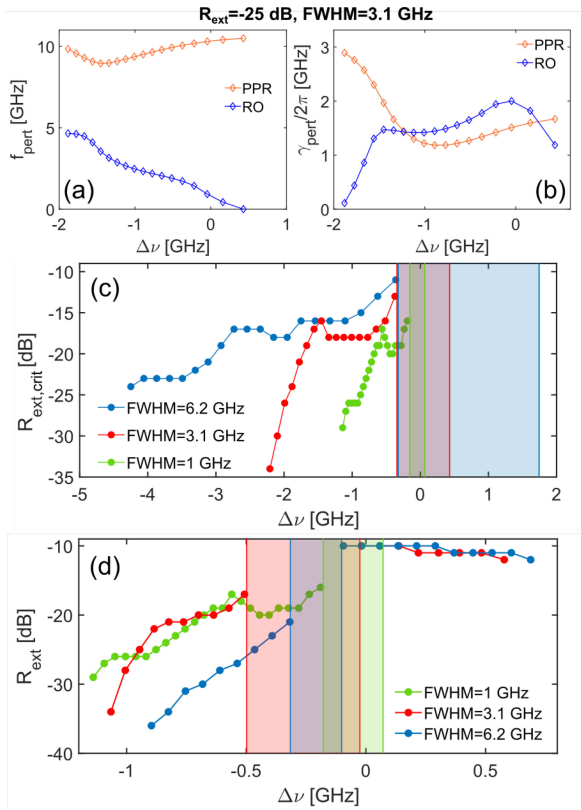
Fig. 5. (a) Frequency and (b) damping of the main system eigenvalues for FWHM = 3.1 GHz and $R_{ext} = -25$ dB as function of the detuning $\Delta\nu$ of the lasing mode. (c) Critical feedback level as a function of the detuning at different reflectivity FWHMs. The effective lengths are 0.73 cm, 1.3 cm, and 3.6 cm for FWHMs of 6.2 GHz, 3.1 GHz, and 1 GHz, respectively. (d) Critical feedback level evaluated at the same effective length ($L_{eff} = 3.6$ cm) for all reflectivity FWHMs (d).

the employment of a QD-DFB can bring feedback tolerance up to -8 dB. To study the impact of optical feedback, we place an external reflector at a distance $L_{ext} = 0.5$ cm from the output coupler in Fig. 1(a), emulating the typical distance in the SiPh circuit from which we expect spurious back-reflections. Based on the origin of the back reflection, we assume that the external optical feedback can range from -40 dB to -10 dB. In Fig. 5 we show the frequency (a) and damping (b) of the two system eigenvalues with the largest perturbation growth rate, as functions of the detuning $\Delta\nu$ for the case of FWHM=3.1 GHz and $r_{ext}^2 = R_{ext} = -25$ dB. The blue eigenvalue is associated to RO and the orange eigenvalue is associated to PPR. Here, while the laser is still stable, PPR has become less damped in comparison to ROs in the main central region for -1.2 GHz$< \Delta\nu < 0.16$ GHz and, in presence of external optical feedback, will eventually trigger instability of the single-mode emission. This is shown in Fig. 5(c), where we report the critical feedback level (i.e., the value of R_{ext} for which the laser becomes unstable) obtained from LSA of (4a)–(4d), for $r_R(\nu)$ given by (3), as a function of the detuning of the lasing frequency for the 3 FWHMs already considered in Fig. 4 (dynamical simulations produce very similar results). The shaded areas of matching colors identify regions of ultra-stability, where the laser is particularly resilient to optical feedback up to $R_{ext} = -10$ dB. This ultra-stability

occurs approximately near the peak of high damping of the RO perturbation in the solitary laser case (see Fig. 3)(b)). In all cases, near the ultra-stable region, instability with $R_{ext} < -10$ dB is triggered by PPR: in particular, smaller FSR for narrow mirror bandwidth favor longitudinal mode coupling and this leads to a lower tolerance to optical feedback. We highlight that this effect is not possible to capture through a standard single-mode Lang-Kobayashi approach [6]. It is important to stress here that Fig. 5(c) evaluates the impact of the external feedback on 3 different lasers having mirrors of different bandwidths but also different effective lengths (since narrow band mirrors due to higher-Q rings have, as a consequence, also longer effective lengths). For this reason, we can say that all mirrors, having bandwidths comparable or smaller than the RO frequency, can properly damp the RO when the laser operates around $\Delta\nu = 0$ GHz and therefore can provide an ultra-high stability, due to the ultra-damped RO and the damped PPR. For more negative $\Delta\nu$, we can state that the laser would be ultra-stable if the RO was the only instability mechanism, but, as clearly evidenced by these results, it is the undamping of the PPR that limits the ultra-high stability. In order to isolate the role of the reflectivity FWHM on the laser stability, we performed a LSA of the model for the same reflectivity bandwidths at fixed effective length L_{eff} (i.e., same FSR) similarly to what was done in [8]. This can be achieved by including an additional piece of waveguide of variable length in the SiPh circuit before the splitter in Fig. 1(a). For this study we choose the effective length of the SiPh mirror for FWHM=1 GHz in Fig. 5(c), which is $L_{eff} = 3.64$ cm. In Fig. 5(d) we show the critical feedback level versus lasing frequency detuning resulting from this analysis. We can observe that, while there is no significant increase of the critical feedback level between FWHM=1 GHz (green curve) and FWHM=3.1 GHz (red curve), the laser feedback tolerance for FWHM=6.2 GHz (blue curve) has drastically decreased in comparison. This suggest, similarly to what was concluded in [8], that lasers with the same FSR but different mirror bandwidths are more resilient to spurious back-reflections when narrower FWHMs are considered. The reason why this is not observe for the red and green curves may be due to the fact that narrow $|r_{eff}|^2$ also imply a higher nonlinearity in the reflectivity phase which in turn reduces the range of accessible lasing modes (as we clearly observe in Fig. 5(d) for the green curve).

V. CONCLUSION

We investigated the CW stability of a III-V hybrid laser. We showed that detuning the lasing frequency with respect to the narrow band mirror reflectivity peak allows to observe regimes of ultra-damped relaxation oscillations, self-pulsing, and quasi-turbulent dynamics and we have detailed the physical mechanisms giving rise to CW instability. In order to properly describe these regimes we showed that it is necessary to account for the narrow band SiPh mirror reflectivity in the model. While narrow mirror bandwidths are effective in suppressing ROs, the emergence of a second resonance due to mode competition leads to lower laser feedback tolerance. Consequently, proper

design of the SiPh mirror is necessary to guarantee the laser feedback tolerance while reducing the mirror bandwidth, which is important in light of enabling isolator-free operation [19], [20].

REFERENCES

[1] C. G. Littlejohns *et al.*, "CORNERSTONE's silicon photonics rapid prototyping platforms: Current status and future outlook," *Appl. Sci.*, vol. 10, no. 22, 2020, Art. no. 8201. [Online]. Available: https://www.mdpi.com/2076-3417/10/22/8201

[2] T. Komljenovic, S. Srinivasan, E. Norberg, M. Davenport, G. Fish, and J. E. Bowers, "Widely tunable narrow-linewidth monolithically integrated external-cavity semiconductor lasers," *IEEE J. Sel. Topics Quantum Electron.*, vol. 21, no. 6, pp. 214–222, Nov./Dec. 2015.

[3] Y. Fan, R. E. M. Lammerink, J. Mak, R. M. Oldenbeuving, P. J. M. van der Slot, and K.-J. Boller, "Spectral linewidth analysis of semiconductor hybrid lasers with feedback from an external waveguide resonator circuit," *Opt. Exp.*, vol. 25, no. 26, pp. 32767–32782, Dec. 2017. [Online]. Available: http://www.opticsexpress.org/abstract.cfm?URI=oe-25-26-32767

[4] D. Huang *et al.*, "High-power sub-kHz linewidth lasers fully integrated on silicon," *Optica*, vol. 6, no. 6, pp. 745–752, Jun. 2019. [Online]. Available: http://www.osapublishing.org/optica/abstract.cfm?URI=optica-6-6-745

[5] M. A. Tran, D. Huang, and J. E. Bowers, "Tutorial on narrow linewidth tunable semiconductor lasers using Si/III-V heterogeneous integration," *APL Photon.*, vol. 4, no. 11, 2019, Art. no. 111101. [Online]. Available: https://doi.org/10.1063/1.5124254

[6] L. Columbo, J. Bovington, S. Romero-Garcia, D. F. Siriani, and M. Gioannini, "Efficient and optical feedback tolerant hybrid laser design for silicon photonics applications," *IEEE J. Sel. Topics Quantum Electron.*, vol. 26, no. 2, Mar./Apr. 2020, Art. no. 8301210.

[7] J. Mak *et al.*, "Linewidth narrowing via low-loss dielectric waveguide feedback circuits in hybrid integrated frequency comb lasers," *Opt. Exp.*, vol. 27, no. 9, pp. 13307–13318, Apr. 2019. [Online]. Available: http://www.osapublishing.org/oe/abstract.cfm?URI=oe-27-9-13307

[8] C. Rimoldi, L. L. Columbo, J. Bovington, S. Romero-García, and M. Gioannini, "Damping of relaxation oscillations, photon-photon resonance, and tolerance to external optical feedback of III-V/SiN hybrid lasers with a dispersive narrow band mirror," *Opt. Express*, vol. 30, no. 7, pp. 11090–11109, Mar. 2022. [Online]. Available: http://opg.optica.org/oe/abstract.cfm?URI=oe-30-7-11090

[9] E. Detoma, B. Tromborg, and I. Montrosset, "The complex way to laser diode spectra: Example of an external cavity laser strong optical feedback," *IEEE J. Quantum Electron.*, vol. 41, no. 2, pp. 171–182, Feb. 2005.

[10] C. Xiang, P. A. Morton, and J. E. Bowers, "Ultra-narrow linewidth laser based on a semiconductor gain chip and extended Si_3N_4 Bragg grating," *Opt. Lett.*, vol. 44, no. 15, pp. 3825–3828, Aug. 2019. [Online]. Available: http://opg.optica.org/ol/abstract.cfm?URI=ol-44-15-3825

[11] L. Chrostowski and M. Hochberg, *Silicon Photonics Design: From Devices to Systems*. Cambridge, U.K.: Cambridge Univ. Press, 2015.

[12] B. Tromborg, H. Olesen, X. Pan, and S. Saito, "Transmission line description of optical feedback and injection locking for Fabry-Perot and DFB lasers," *IEEE J. Quantum Electron.*, vol. 23, no. 11, pp. 1875–1889, Nov. 1987.

[13] P. Bardella and I. Montrosset, "A new design procedure for DBR lasers exploiting the photon-photon resonance to achieve extended modulation bandwidth," *IEEE J. Sel. Topics Quantum Electron.*, vol. 19, no. 4, Jul./Aug. 2013, Art. no. 1502408.

[14] U. Feiste, "Optimization of modulation bandwidth in DBR lasers with detuned Bragg reflectors," *IEEE J. Quantum Electron.*, vol. 34, no. 12, pp. 2371–2379, Dec. 1998.

[15] L. A. Coldren and S. W. Corzine, *Semiconductor and Photonic Integrated Circuits*. Hoboken, NJ, USA: Wiley, 1995.

[16] C. Xiang, P. A. Morton, J. Khurgin, C. Morton, and J. E. Bowers, "Widely tunable Si_3N_4 triple-ring and quad-ring resonator laser reflectors and filters," in *Proc. IEEE 15th Int. Conf. Group IV Photon.*, 2018, pp. 1–2.

[17] P. A. Morton, C. Xiang, J. B. Khurgin, and J. E. Bowers, "Ultra-low noise semiconductor lasers," in *Proc. Conf. Lasers Electro- Opt.*, 2022.

[18] J. Mork, Y. Yu, T. S. Rasmussen, E. Semenova, and K. Yvind, "Semiconductor Fano lasers," *IEEE J. Sel. Topics Quantum Electron.*, vol. 25, no. 6, Nov./Dec. 2019, Art. no. 2900314.

[19] Y. Matsui, R. Schatz, D. Che, F. Khan, M. Kwakernaak, and T. Sudo, "Low-chirp isolator-free 65-GHz-bandwidth directly modulated lasers," *Nature Photon.*, vol. 15, no. 1, pp. 59–63, 2021.

[20] Z. Zhang, D. Jung, J. C. Norman, W. W. Chow, and J. E. Bowers, "Linewidth enhancement factor in InAs/GaAs quantum dot lasers and its implication in isolator-free and narrow linewidth applications," *IEEE J. Sel. Topics Quantum Electron.*, vol. 25, no. 6, Dec. 2019, Art. no. 1900509.

[21] L. Tang, J. Li, S. Yang, H. Chen, and M. Chen, "A method for improving reflection tolerance of laser source in hybrid photonic packaged micro-system," *IEEE Photon. Technol. Lett.*, vol. 33, no. 9, pp. 465–468, May 2021.

[22] M. Matsuda *et al.*, "Low-noise characteristics on 1.3-μm-wavelength quantum-dot DFB lasers under external optical feedback," in *Proc. IEEE Int. Semicond. Laser Conf.*, 2018, pp. 1–2.